Chemical imaging of the stratum corneum under controlled humidity with the attenuated total reflection Fourier transform infrared spectroscopy method

K. L. Andrew Chan
Sergei G. Kazarian
Imperial College London
Department of Chemical Engineering
London, SW7 2AZ, United Kingdom

Abstract. Attenuated total reflection Fourier transform infrared spectroscopic imaging was applied to study human stratum corneum (SC) tissue, the outermost layer of the skin. This imaging approach was combined with a controlled environment cell to demonstrate the possibility of obtaining chemical images of SC exposed to a wide range of relative humidities and diffusion of ethanol through the SC tissue with a specially designed liquid cell. The effect of water vapor sorbed into the SC on the distribution of other components in the SC was studied. Principal component analysis was applied in conjunction with univariate analysis to differentiate the distribution of different components in the SC. Swelling of the SC, a heterogeneous distribution of natural moisturizing factor and water, was detected upon the increase of relative humidity. The approach to image the penetration of liquid ethanol into the SC was also demonstrated and showed good potential and implications for studying transdermal drug delivery. *© 2007 Society of Photo-Optical Instrumentation Engineers.* [DOI: 10.1117/1.2754686]

Keywords: skin surface; water sorption; transdermal drug delivery; Fourier transform infrared spectroscopy; multivariate analysis.

Paper 07034R received Jan. 25, 2007; revised manuscript received Mar. 15, 2007; accepted for publication Mar. 17, 2007; published online Jul. 16, 2007.

1 Introduction

Hydration of skin plays an important role for the function of skin as a barrier for the human body.[1] The amount of water present in stratum corneum (SC), the outermost layer of the skin, affects the barrier properties of skin. Hydration of SC is crucial for the appearance and flexibility of skin, is important for transdermal delivery, and plays a key role in cosmetic treatment of skin and the applications of many healthcare products to skin. The effect of different topical formulations and medications relies on their moisturizing effect, which often enhances their performance.

A number of techniques have been developed to analyze the amount of moisture in the SC and to study the distribution of water within the SC. Some of the main techniques to study the hydration of SC are electrical methods that measure the effect of water present on the conductance or capacity of SC.[2,3] However, the use of these techniques is not straightforward, as the dependency of the electrical properties of water on the amount of water may be highly nonlinear. Furthermore, applications of electrical methods cannot easily differentiate between the effect of water and other constituents present in topical formulations.[4] Due to its intrinsic chemical specificity, vibrational spectroscopy (infrared and Raman) provides an opportunity not only to measure the amount of water in the SC but also to differentiate the presence and behavior of other molecules in the SC and to analyze the effect of water on changes in the SC. Thus, a very interesting application of confocal Raman spectroscopy[5] revealed the depth concentration profile of water as a function of the distance from the surface of the skin. This approach led to the successful development of instrumentation by River Diagnostics for noninvasive *in vivo* measurements of skin. Xiao and Imhof have demonstrated the use of opto-thermal radiometry to obtain depth distribution of water in SC *in vivo*.[6] Recently, a method of magnetic resonance profiling using gradient at right angles to the field has been applied to study the moisture content in skin tissue.[7,8] These results provided opportunities for *in vivo* measurement of skin hydration. However, these approaches typically provide chemical information along the line perpendicular to the surface of the skin and lack imaging capability. The averaged information obtained in confocal Raman measurements originates from the measured confocal volume (with dimensions of a few micrometers). It is possible to obtain such information as a function of depth from several locations on the surface of the skin, but this would require a significant amount of time (hours) and the information cannot be obtained simultaneously.

Near-IR imaging provides a possibility to image the effect of hydration at different locations in the sample simultaneously in a relatively large area of skin,[9] but the near-IR approach lacks the chemical specificity of infrared spectroscopy in the mid-IR region, which can easily differentiate between functional chemical groups and their interactions. This is because near-IR relies on the spectral bands corresponding

Address all correspondence to S. G. Kazarian, Tel: +44 207 5945574; E-mail: s.kazarian@imperial.ac.uk.

1083-3668/2007/12(4)/044010/10/$25.00 © 2007 SPIE

to overtones or combination transitions, while the mid-IR spectroscopy primarily deals with fundamental transitions. The depth of penetration of near-IR spectroscopy is also less well defined, which causes additional difficulties for quantitative analysis. The combination of the high chemical specificity of Fourier transform infrared (FTIR) spectroscopy with the high-speed imaging capability offered by the focal plane array detector[10,11] enabled the development of a variety of applications in a number of research fields including imaging of biomaterials[12] and biological tissues.[13,14] FTIR spectroscopy with the attenuated total reflection (ATR) approach requires a minimal sample preparation method because of the relatively small depth of penetration (a fraction of a micrometer to a few micrometers) of the evanescent wave that probes into the sample.[15] Our group has developed a range of ATR-FTIR measurement approaches for imaging with different spatial resolutions and fields of view for different applications,[16–18] while Varian has a patent on the imaging ATR spectrometer.[19] We have demonstrated the feasibility of studying pharmaceutical samples under controlled environments using FTIR imaging by incorporating a controlled environment cell with an ATR accessory.[20] The suitability of ATR-FTIR imaging for *in situ* studies of biological samples has been demonstrated previously.[14,16] There are opportunities in applying ATR-FTIR imaging in the mid-IR region to skin tissue exposed to controlled humidity to study the hydration of skin.

In this paper, the absorption of water in human stratum corneum exposed to a large range of controlled relative humidities (from a very dry to a very humid atmosphere) has been measured with the diamond ATR-FTIR imaging method to demonstrate the potential of this approach to study human SC tissue under controlled environments *in situ*. A new liquid cell for studying diffusion of different components from solution through the SC tissue has also been introduced. Principal component analysis (PCA) was found to be a useful tool to extract images that represent the distribution of different components that are otherwise difficult to generate by the univariate method.[21,22] This study used PCA to analyze the obtained imaging data sets and to validate images produced with the univariate approach.

2 Materials and Methods

The controlled humidity cell (VGI 2000M, Surface Measurement System Ltd., UK) was designed to be used in transmission spectroscopic measurements with a microscope, and it was described in detail in Ref. 23. The range of relative humidity (RH) inside this cell can be varied between 3% and 95% and can be operated at temperatures in the range from 15 to 40°C. Room temperature (22°C) was used for all experiments shown in this study.

Human SC samples of ca. 15–20 μm thick, supplied by the London School of Pharmacy (LSP) (originally supplied by UKHTB with the appropriate ethics approval), were extracted from human cadaver skin from abdominal tissue and were fixed and attached on a foil and stored in a freezer before use. The sample was defrosted at room temperature (22°C), and the surface was gently cleaned with ethanol. There is no apparent ice damage to the SC tissue observed under a visible light microscope. A previous study has shown that this freezing procedure does not alter the SC barrier function.[24] The sample with foil was then immersed in deionized water until the SC was detached from the foil surface and floated. The floating skin was carefully transferred to the diamond ATR crystal measuring the surface where it was positioned to the center and lay flat with the epidermal side facing the crystal. Excess water was removed and the sample was dried overnight with the aid of the controlled humidity cell at 3% RH (the lowest humidity available). The sample was then exposed to a controlled RH. The water content in the sample was monitored every hour by the measurement of the imaging spectral data sets during the exposure of the sample in the controlled environment. It has been found that three hours was the minimum time required for the water content in the tissue to equilibrate with the controlled environment. Each time when the RH was adjusted, the sample was therefore allowed to equilibrate in the controlled environment for at least three hours before a new imaging measurement was commenced. Preliminary measurements in this study have shown that the water content in the equilibrated SC tissues did not vary significantly in the range of RH between 3% and 50%; therefore, images were acquired when the sample was equilibrated at RH of 3%, 50%, 65%, 80%, and 95%. Several experiments have been performed in each case to ensure the reproducibility of the results.

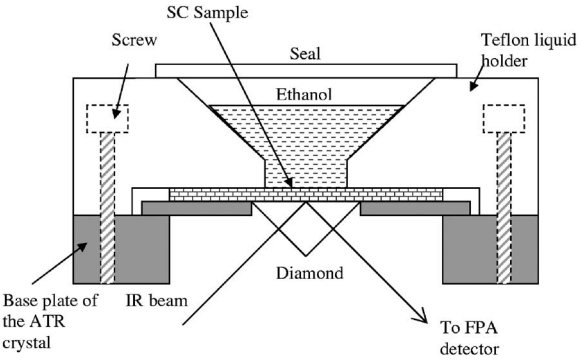

Fig. 1 Schematic diagram for the liquid holder for the *in situ* measurement of ethanol in contact with SC tissue.

For the experiment with ethanol, liquid ethanol (99.6% pure) was placed on the surface of the SC for the *in situ* measurement instead of covering the diamond ATR surface with the controlled humidity cell. A liquid cell, shown in Fig. 1, has been manufactured specifically for the *in situ* experiments on the penetration of liquids through the human SC in the way that liquid diffuses into the SC from the top surface of the SC but not from the interface between the ATR crystal and the tissue. The SC tissue was prepared similarly to the humidity experiment, but, in this case, it was dried under room condition (22°C, 40% RH) instead of 3% RH. The liquid holding cell was introduced on the top surface layer of the SC tissue after it was dried, and leakage of liquid was prevented by holding down the cell with screws (see Fig. 1). Ethanol was added followed by a series of measurements. A seal was introduced to the top of the cell to prevent the ethanol from evaporating.

FTIR images were collected with a continuous-scan spectrometer equipped with a large sample compartment and a 64×64 focal plane array (FPA) detector. A 128×128 FPA

detector was also used in some of the measurements to obtain a larger field of view. A diamond ATR accessory (Golden Gate, Specac Ltd., UK) was used providing a field of view of ca. $500 \times 700\ \mu m^2$ with the 64×64 FPA detector and ca. $900 \times 1260\ \mu m^2$ with the 128×128 FPA detector. It is important to note that the 64×64 FPA detector, used in this study, is different from those used in most of our other studies described in previous publications (e.g., Refs. 16, 25, and 26), thus providing a smaller field of view when it is used with the same accessory. The diamond ATR accessory was not specifically designed for imaging purpose, but it has been shown to be a versatile ATR imaging tool.[16] A spectral resolution of 8 cm^{-1} has been used in this study, 100 scans (which took ca. 200 s) were collected using the 128×128 FPA, and 20 scans were used using the 64×64 FPA detector to reduce the scanning time to ca. 20 s (i.e., ca. 1 s per scan). PCA and spectral preprocessing were performed using the ISys software (Spectral Dimension/Malvern).

3 Results and Discussion

For any ATR measurements, a good contact between the sample and the ATR crystal is very important for obtaining reliable data. Ideally, the sample should self-adhere to the ATR measuring surface. Unlike the studies with polymers or pharmaceutical samples, it was not possible to melt or cast the SC tissue from a solution of organic solvent, as this would destroy the morphology of the original sample. Pressing the sample with a press is also not desirable as the surface of the SC tissue should be free from any blockage for the access of liquid or vapor to be studied. A previous study using the ATR imaging approach with SC and other biological tissues using the ATR approach has shown that these tissues would self-adhere to the ATR crystal surface.[14,27] By floating the SC sample and ensuring that no air bubbles are trapped between the sample and water, followed by removing the water underneath the SC, a good contact between the SC and the ATR crystal has been ensured. However, reliable ATR imaging measurements also require this contact to be homogeneous. In the case of a heterogeneous sample, it is often not easy to identify any possible heterogeneity of optical contact from the variation of absorbance because the absorbance at any particular wavenumber in a spectrum is also a function of the component concentration (composition). Ekgasit[28] has shown that comparing the absorbance of the same spectral band measured using the p- and s-polarized light allows one to assess the quality of optical contact between the sample and the crystal. A similar test has been performed with the sample of SC dried on the diamond crystal, and the uniformity of the sample–crystal contact has been assessed. Since it was difficult to compare all 4096 spectra measured with p-polarized light with the spectra measured with s-polarized light, a ratio of the absorbance of the bands measured with different polarization in the high wavenumber region, where it is the most sensitive to the size of any possible gap between the sample and the crystal, has been used for the comparison. The ratio of the absorbance of the ν (NH) band at 3280 cm^{-1} measured with s- and p-polarizations has been calculated and is shown in Fig. 2. For an intimate optical contact and an angle of incidence of 45 deg, this ratio should be 2. The image shown in Fig. 2 shows that this ratio is ca. 1.8, which means that the sample preparation method employed in this study results in a gap of insignificant size (thickness$<0.01\ \mu m$) between the ATR crystal and the sample. The lack of variation of this ratio across the imaged area confirms that the contact is uniform. A recent FTIR imaging study of SC tissue using a variable-angle ATR accessory has also shown that the contact between the SC tissue and the ATR crystal-measuring surface is homogeneous over the imaged area.[29]

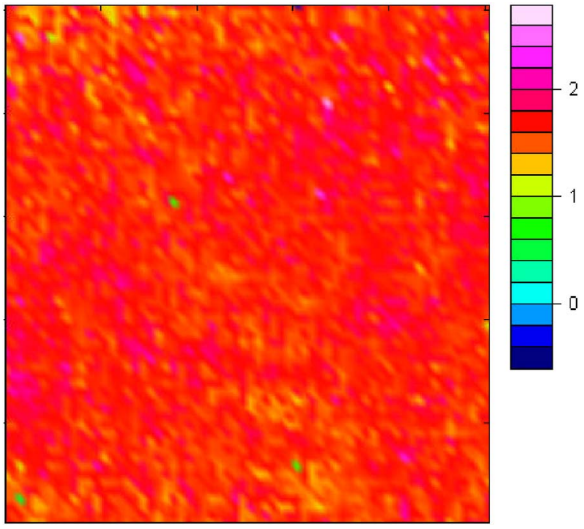

Fig. 2 Image resulting from the ratio between the p- and s-polarized spectral absorbance of the NH stretch band at 3280 cm^{-1} of the prepared SC tissue on the diamond ATR crystal.

3.1 *Skin Under Controlled Humidity*

After the sample was dried overnight on the ATR crystal with the controlled humidity cell set to 3% RH, an FTIR image was measured. The peak area of the Amide II band of protein between 1565 cm^{-1} and 1500 cm^{-1} of all spectra measured was integrated and used to plot a map showing the distribution of protein in the skin. The Amide II band was used instead of the Amide I band (1642 cm^{-1}) because of the possible overlap with the band of water bending mode (at ca. 1640 cm^{-1}). The image shown in Fig. 3 demonstrates that the surface of the studied sample of SC is heterogeneous. There are clear domains of low protein concentration. Spectra extracted from the red and green areas of the images showing the distribution of protein-rich areas (top row) are shown in Fig. 4. The low-protein-concentration areas have also shown some absorbance in the 1745 cm^{-1} region. A similar observation has been made before, and this absorbance was assigned to the presence of the lipid-rich domains on the surface of the SC.[16] These lipid-rich domains are probably the remains of the nonpolar sebaceous lipids of the surface.[30] The plot of the distribution of the band at 1743 cm^{-1} (the integration range used was 1767 cm^{-1} to 1720 cm^{-1}) has produced images showing the distribution of lipids that were complementary to the corresponding images of the distribution of proteins (shown in Fig. 3). The distribution of the absorbance of the band at ca. 1400 cm^{-1}, which has been previously assigned to the natural moisturizing factor (NMF, a mixture of proteins constituent amino acids, amino-acid derivatives, and

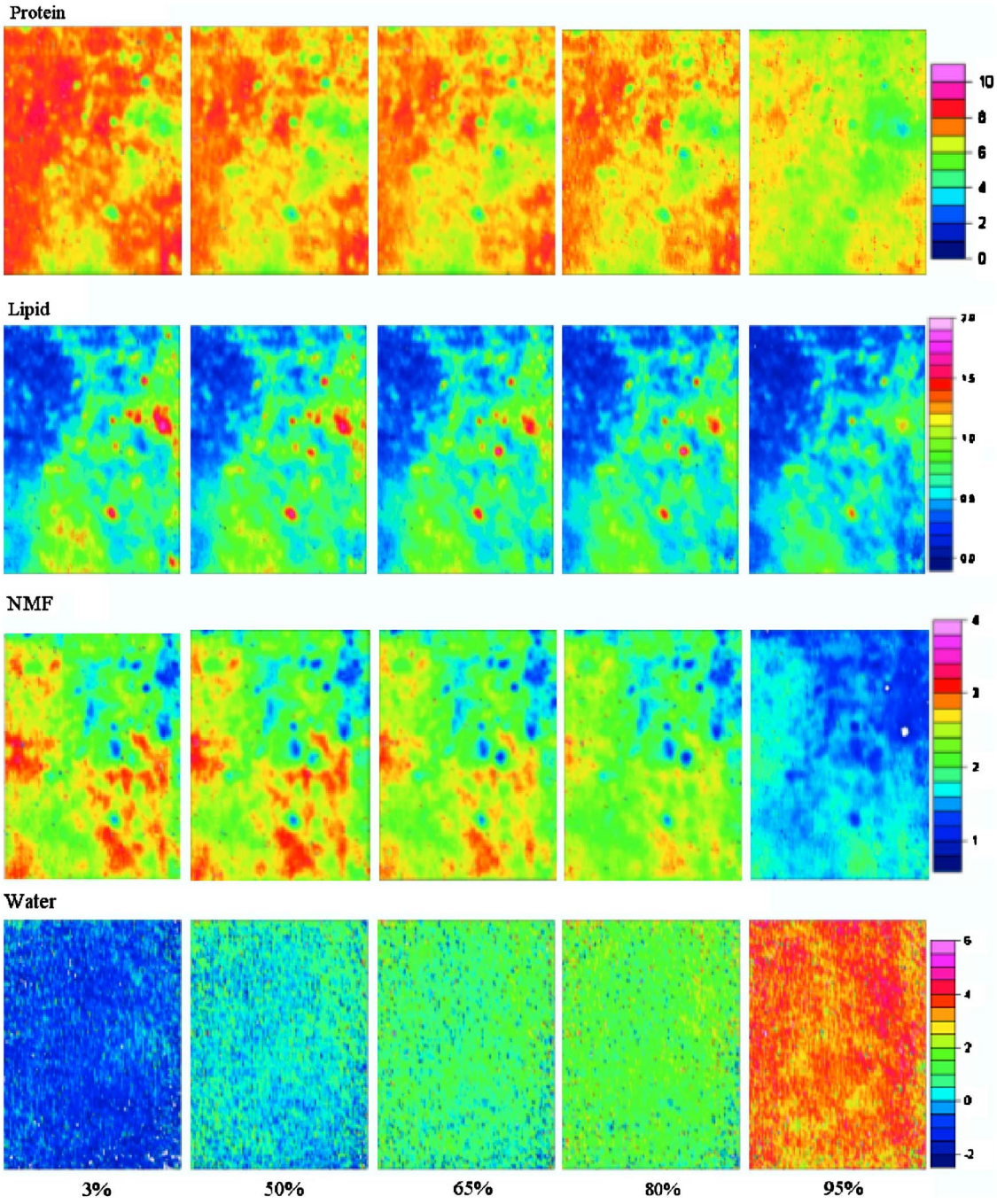

Fig. 3 FTIR images of the SC at different controlled humidities. The images represent the distribution of different components, which are labeled at the top of each row. The color scale at each row has been adjusted to allow direct comparison to be made between images. The humidity levels are shown at the bottom of the images. The image size is approximately 900 μm $\times$ 1260 μm (color online only).

salts),[31,32] is also shown in Fig. 3. The distribution of the NMF was somewhat similar to the distribution of protein in the imaged area, but it was not exactly the same. The heterogeneity of the SC is not limited to the distribution of proteins and lipids as demonstrated by ATR-FTIR imaging, which is a powerful tool for the analysis of biomedical samples.[14] After imaging the relatively dry sample, it was then exposed to 50%, 65%, 80%, and 95% RH. Images showing the distribution of water have been generated by choosing an integration range such that the contribution from the absorbance of the NH stretching band to the OH stretch of water (3640–3550 cm^{-1}) was relatively small. The distribution of proteins and lipids was measured at each humidity level, and the results are shown in Fig. 3. The images in the top row show that when the relative humidity increases, the absorbance of the Amide II band of protein decreases. Water sorption to the protein domains from the controlled environment caused the SC to swell. However, this swelling effect was not very strong when the sample was exposed to RH between 3%

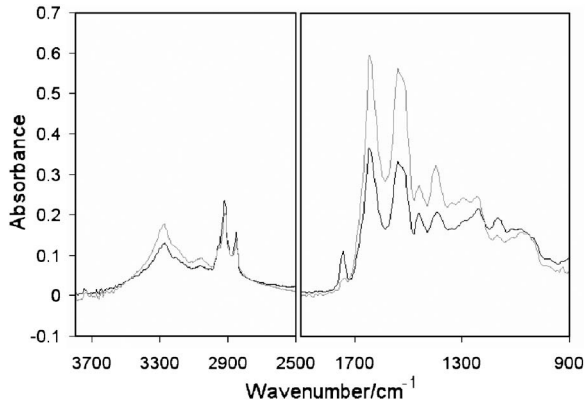

Fig. 4 Spectra extracted from green area (black line) and red area (gray line) of top left image of Fig. 3.

and 80%. In fact, this swelling was not observable for images showing the distribution of proteins in the range of RH between 50% and 80%.

In contrast, images in the bottom row of Fig. 3 (water distribution) have shown that the amount of water was increasing with the increase in RH. Furthermore, the lipid and the NMF have shown a decrease in the overall absorption within this change of RH. All this points to the fact that NMF is more sensitive to the change in humidity (in the range of 50–80%) compared to the protein domains. Unfortunately, there was no direct correlation between the water distribution images and the NMF images. Also, it was very difficult to use the OH stretching band of water to represent its distribution in the univariate analysis because of its overlap with the NH stretching band of protein; hence, the images showing the distribution of water were only qualitative. Nevertheless, a ratio of the images showing the distribution of protein and NMF at the two extreme RHs has been created to normalize the NMF distribution against the protein distribution. The resulting images are shown in Fig. 5. The ratio of the images has shown a similar NMF distribution to the original NMF map shown in Fig. 2 at low RH. At 95% RH, this ratio of the images has shown some difference to the corresponding image shown in Fig. 3 because the ratio of the images depends not only on the distribution of NMF but also on the swelling

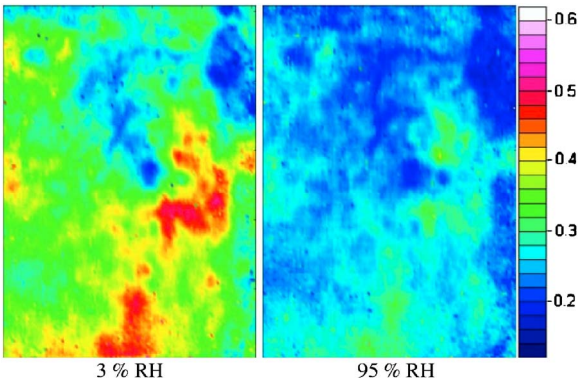

Fig. 5 Image generated by ratioing the NMF distribution to the protein distribution at 3% RH (left image) and 95% RH (right image). The image size is approximately 900 μm $\times$ 1260 μm.

of the SC. In order to obtain images that are more independent from the contribution of different components in the SC tissue, PCA has been applied to analyze the data sets obtained from the sample at 3% RH and 95% RH. The multivariate approach has been demonstrated as a promising data analysis method that can be used to extract information from the large amount of data collected.[21,33–37] However, before carrying out the PCA, second derivative has been applied to all spectra to remove any possible effects of variation of the baseline. The second derivatives are calculated using the Savitsky–Golay polynomial filtering method with a filter length of 7 and a filter order of 3. To remove the contribution from uncompensated CO_2 in the background, only the spectral region, which contains the most information about the contribution of protein and NMF, between 1800 cm^{-1} and 1000 cm^{-1} were used in the PCA. Since all spectral peaks will be pointing downward after taking the second derivative, a multiple of -1 is applied to all spectra to reverse the direction of the peaks for a clearer presentation. The loading and score plots of the results measured from the sample at 3% RH and 95% RH are shown in Figs. 6 and 7. Consider, first, the PCA results from the data measured at 3% RH. Clearly, principal component (PC) 1 describes the protein distribution in the SC, which the score plot has shown similarity to the image of the protein distribution in Fig. 3, and it can be identified by typical protein absorption bands at 1647 cm^{-1} (Amide I) and at 1543 and at 1512 cm^{-1} (Amide II). PC 2 and 3 represent a mixture of uncompensated water vapor, which is marked by the spike's presence in the loading between 1800 and 1400 cm^{-1} and the distribution of lipids, which is indicated by the characteristic carbonyl band at 1745 cm^{-1}. The score plot of PC 4 is, interestingly, the reverse image of the NMF distribution shown in Fig. 3, suggesting that PC 4 is the negative correlation of the NMF. Looking at the loading of PC 4, one can identify the negative bands at ca. 1400, 1339, and 1292 cm^{-1}, which correspond to the spectral features of NMF. Although the loading of PC 5 and 6 showed some spectral features similar to the NMF in the 1400–1300-cm^{-1} region, and the score plot of PC 5 showed some similarity in distribution of the NMF component shown in Fig. 3, they only accounted for 0.09% and 0.06% of the variance of the data set. Hence, PC 5 and 6 were generally regarded as the description of a possible band shift due to slight change in the chemical environment in the heterogeneous SC tissue. Other PCs beyond PC 6 have been disregarded, as the percentage of information contained in these PCs decreased further and their corresponding loadings also became more noise-like.

The loading and the score plots of the PCA of the data, in the fingerprint region, measured at 95% RH are shown in Fig. 7. Similar to the PCA of the data measured at 3% RH, PC 1 describes the distribution of proteins in the SC tissue as shown by the similarity of the loading plot to the protein image presented in Fig. 3 and the presence of the Amide I (1643 cm^{-1}) and Amide II (1543 and 1512 cm^{-1}) spectral features in the loading 1. The slight red shift of the Amide I spectral feature compared to the 3% RH data is a possible result of water molecules interacting with the carbonyl group of the protein.[38] Furthermore, the ratio of the two Amide II peaks showed a significant difference between the data measured at 3% and 95% RH. Amide II has been generally re-

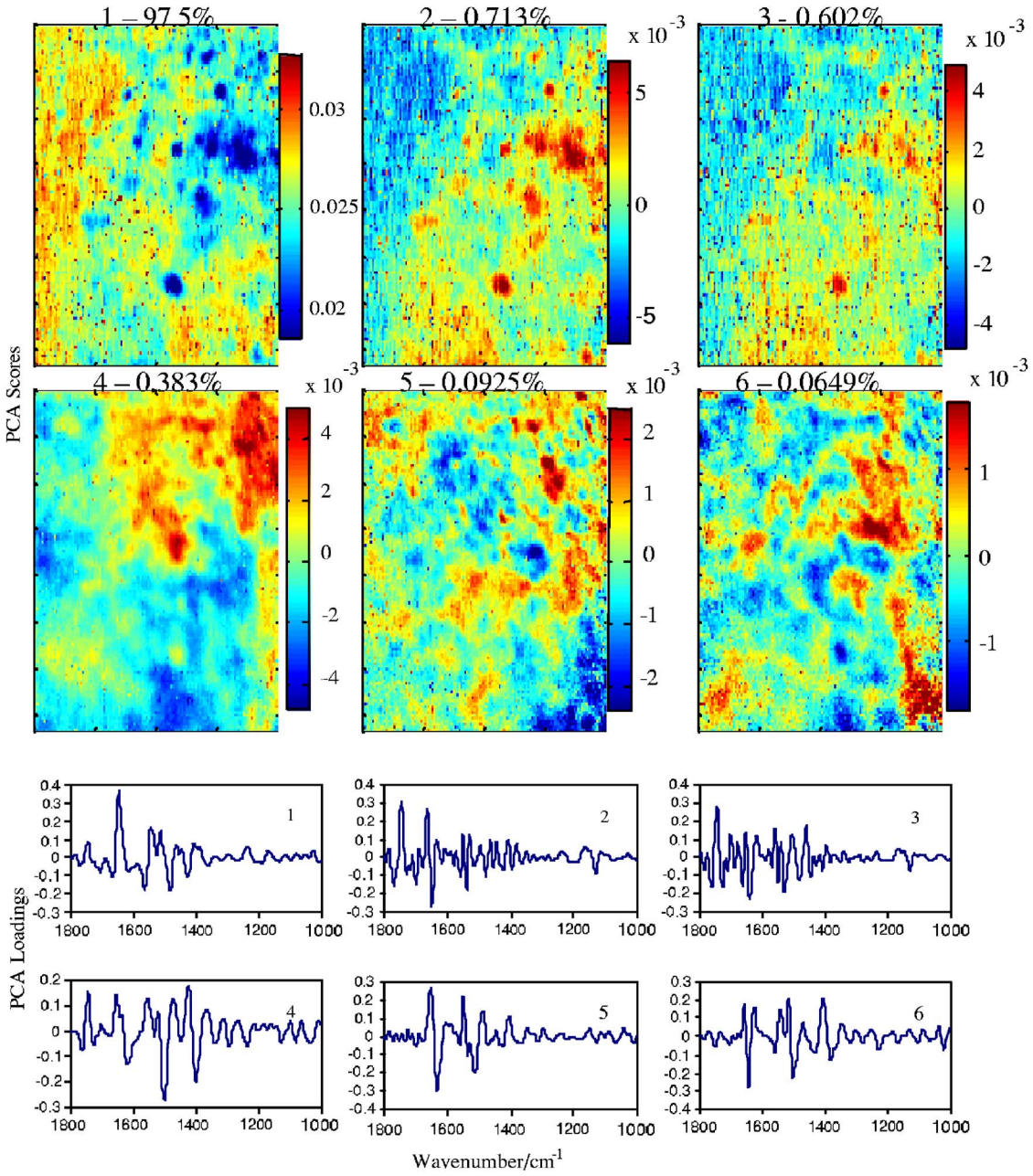

Fig. 6 The first six PC loading and score plots of the ATR-FTIR imaging data in the fingerprint region measured at 3% RH. The number (1–6) represents the PC the plot describes. The percentage represents the proportion of the variance of the data the PC describes.

garded as less structurally sensitive than the Amide I band,[39] and it is often more difficult to interpret. Nevertheless, the analysis of these imaging data sets has demonstrated that it is possible to extract subtle but reliable information from the imaging data. The loading of PC 2 probably describes the uncompensated water vapor and, therefore, the score plot of PC 2 did not show any distribution. PC 3 clearly describes the lipid components in the SC tissue. The loading of PC 3 contains the lipid spectral feature at 1745 cm^{-1} [ν(C═O) band], and the score plot is similar to the image of the distribution of lipids shown in Fig. 3. A closer look at the loading of PC 4 has found spectral features at ca. 1408, 1350, 1330, and 1300 cm^{-1} that belong to NMF. The positions of the bands corresponding to NMF extracted in this case were not exactly the same as those extracted from the PCA of the data measured at 3% RH (Fig. 6) because the chemical environment in the SC tissue could be different with the presence of water molecules. The score plot of PC 4 in Fig. 7 has demonstrated a close match with the image in Fig. 3 that described NMF distribution at 3% RH. It is also complementary to the score plot of PC 4 in Fig. 6. This demonstrates that the distribution of NMF in the SC tissue did not change upon exposure to 95% RH. The similarity between the score plot of PC 4 and the NMF image at 3% RH in Fig. 3 also demonstrates the advantage of PCA over univariate analysis. While apparent differences in NMF distribution have been observed for the

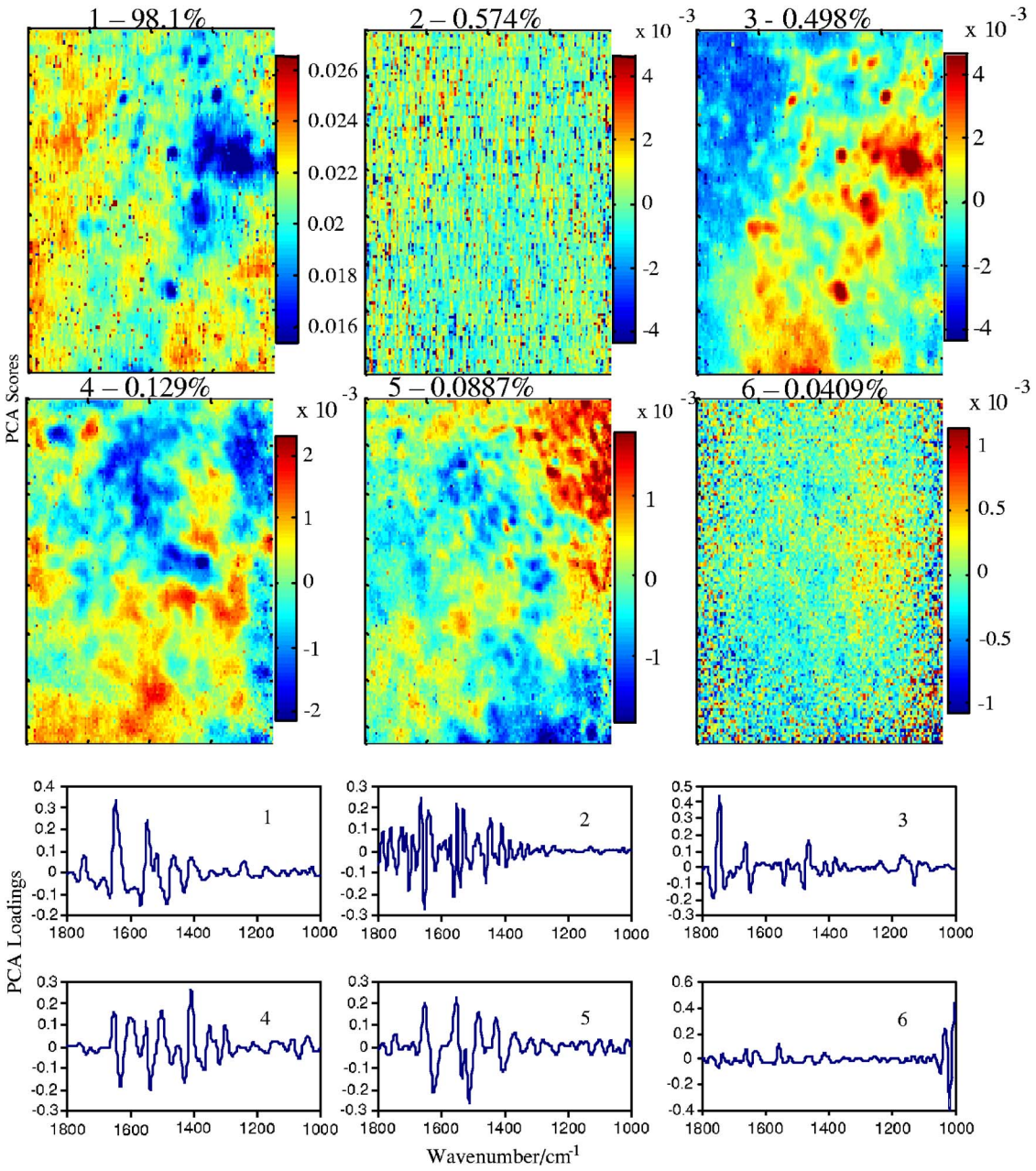

Fig. 7 The first six PC loading and score plots of the ATR-FTIR imaging data in the fingerprint region measured at 95% RH. The number (1–6) represents which PC the plot describes. The percentage represents the proportion of the variance of the data the PC describes.

cases of high and low RH from the images generated by the univariate method (which was probably due to swelling of protein), PCA has demonstrated no significant differences for the distribution of NMF. The loading of PC 5 was generally regarded as the description of a possible band shift due to a slight change in chemical environment in the heterogeneous SC tissue and possibly heterogeneous distribution of water in the SC tissue, which is marked by the loading feature at 1650 cm^{-1}. PC 6 is clearly the remaining noise in the 1000-cm^{-1} region and therefore can be ignored.

Another advantage of the multivariate approach over the univariate method is that it can identify the distribution of components with spectral features that overlap with other components. The integral range used for generating the image representing the distribution of water in Fig. 3 utilizes only part of the broad ν(O–H) stretching band of water. The images generated may be affected by the change in band shape in this region due to the differences in the chemical environment at different composition and the protein NH stretching band. PCA was applied to the region between 3750 and 2750 cm^{-1}. Instead of taking the second derivative of all spectra, a simple two-point baseline correction (one at the beginning and one at the end of the spectral range) has been applied because the second derivative will remove the broad spectral feature of the ν(O–H) stretching band of water. The

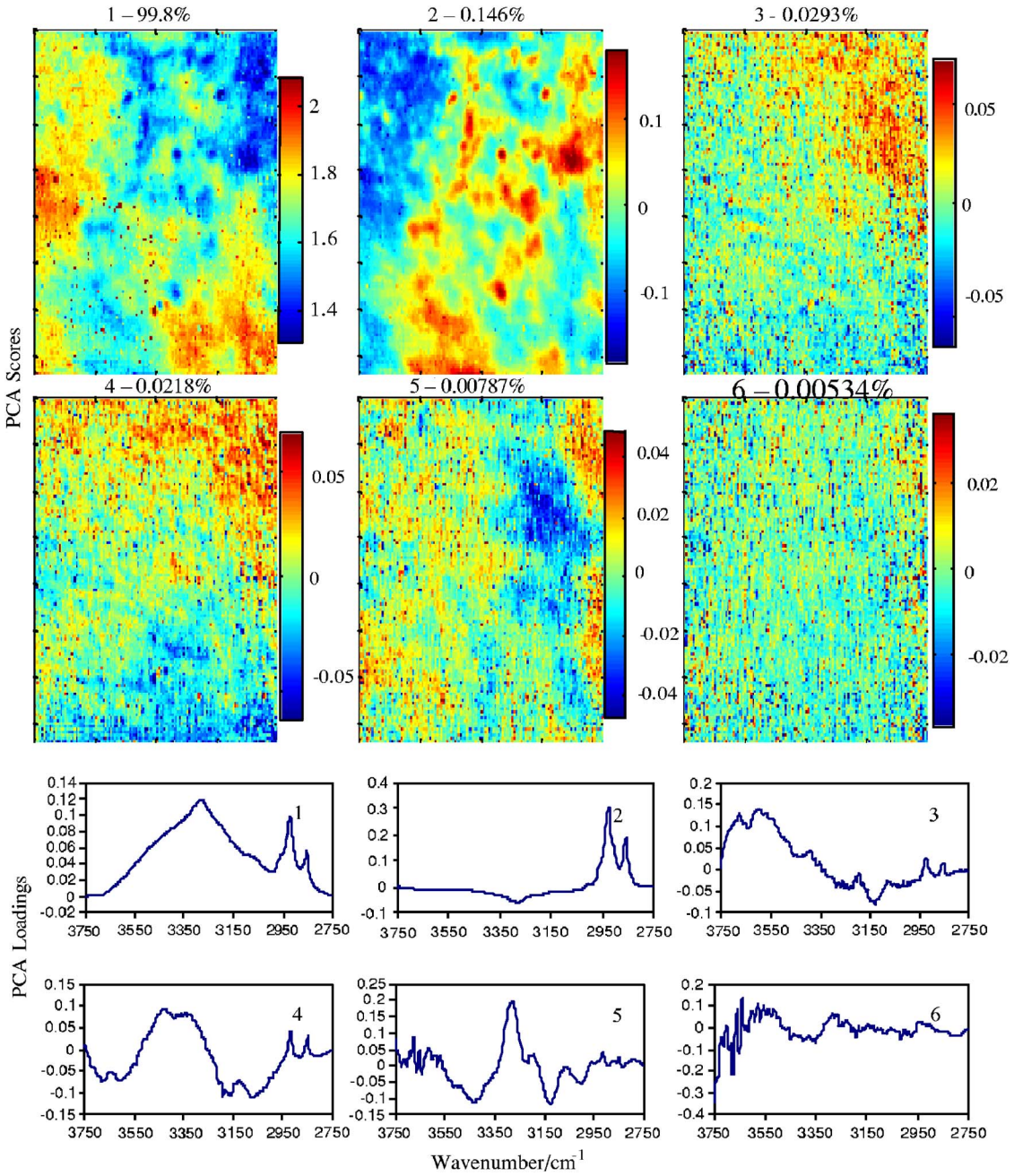

Fig. 8 The first six PC loading and score plots of the ATR-FTIR imaging data in the CH–NH stretch absorption band region measured at 95% RH. The number (1–6) represents which PC the plot describes. The percentage represents the proportion of the variance of the data the PC describes.

results are shown in Fig. 8. PC 1 and 2 describe the proteins and the lipids of the SC and their distribution. PC 3 and PC 4 have positive spectral feature in the loading in the 3600-cm^{-1} and 3380-cm^{-1} region, showing evidence of heterogeneous water distribution in the SC tissue at 95% RH. The spatial distribution of water is described in the corresponding score plot shown in Fig. 8. It is interesting to note that PCA enhances the image showing the distribution of water, which is demonstrated by comparison of the PC 4 in Fig. 8 to the imaging of water distribution in the sample measured at 95% RH in Fig. 3. This also demonstrates the potential of the ATR-FTIR imaging technique to study the distribution of water in SC tissue under different conditions. The score plot of PC 5 is complementary to the score plot of PC 4 in Fig. 7, which has been interpreted as the distribution of NMF. It has been shown that it is possible to extract similar information by performing PCA to different parts of the spectrum separately. PC 6 did not show any important information, as demonstrated by the relatively featureless loading and the score plots.

3.2 *Skin Exposed to Liquid Ethanol*

The second experiment conducted in this study was the penetration of ethanol through the SC of human skin as a function

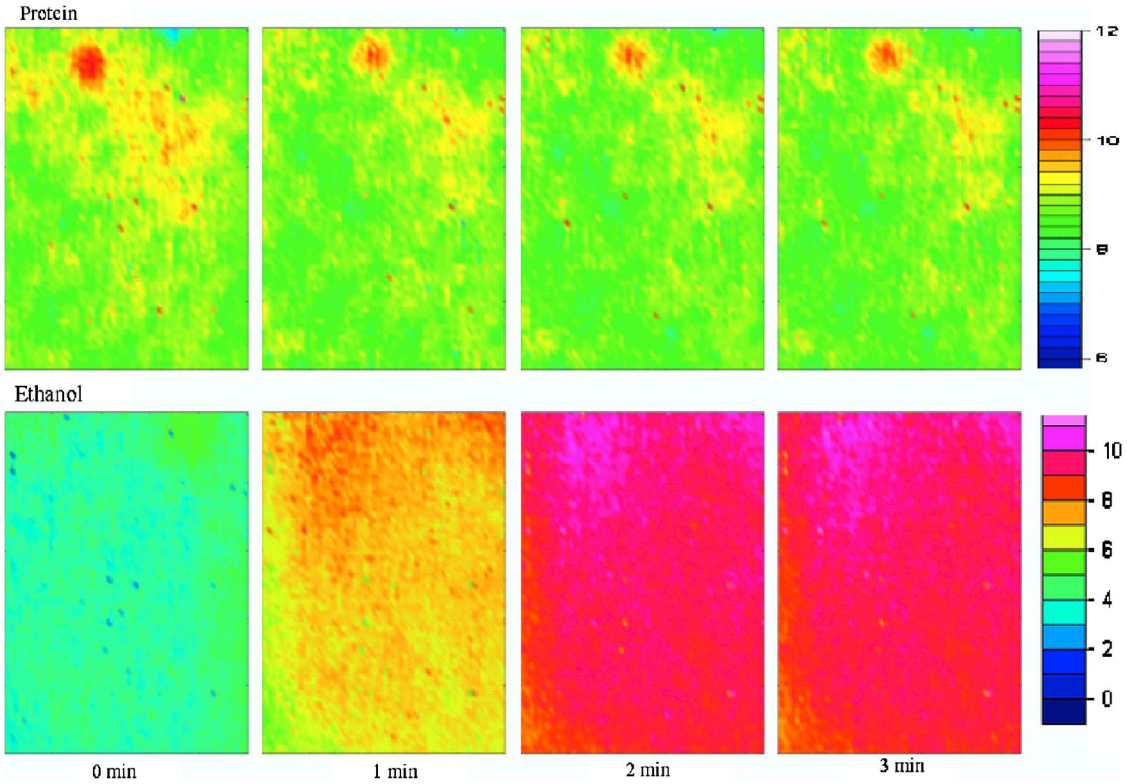

Fig. 9 FTIR images of protein (1565–1500 cm^{-1}) and ethanol (1100–1000 cm^{-1}) distribution at different times after the addition of ethanol to the surface of the SC tissue. The image size is approximately 500 $\mu m \times 700$ μm.

of time using the ATR-FTIR imaging approach. Solutions in ethanol are often used in formulations for skin treatment. For example, the effect of ethanol on transport of drug through the model polymer membranes was analyzed previously using FTIR imaging.[40]

In this experiment, instead of covering the SC tissue with the controlled humidity cell, which can be used to generate organic solvent vapor with different partial pressures,[41] the new cell specifically designed for retaining liquid on the diamond surface was used to contain the ethanol on the skin surface. The images showing the distribution of different components that were measured immediately after ethanol has been introduced are presented in Fig. 9. The same univariate method that was used to generate the images in the controlled humidity experiment was applied. The bands at 1086 cm^{-1} and 1046 cm^{-1} have been used to represent the presence of ethanol (the integration range used was 1100–1000 cm^{-1}). A 64×64 FPA detector was used in this experiment because a smaller array would allow a shorter scanning time and, hence, a higher temporal resolution. The results shown in Fig. 9 have demonstrated that ethanol penetrated into the SC in a very short time (the equilibrium concentration of ethanol in SC was reached within 2 min). The protein domains swell slightly, which is marked by the small decrease of absorbance of the Amide I band. Although the distribution of proteins appears to be heterogeneous, the sorption of ethanol seems to be relatively homogeneous (within the spatial resolution used), which could mean that the permeation of ethanol through the skin was not affected by the heterogeneous nature of the SC layer.

4 Conclusions

The combination of ATR-FTIR imaging with a controlled environment cell allowed us to obtain chemical images of the surface of stratum corneum (SC) under controlled relative humidity. It has been shown that FTIR imaging provides information on swelling of SC as a function of humidity. The SC tissue swells more significantly when the RH increases from 80% to 95% than when it changes from 3% to 80%. The amount of water sorption into SC increased with the increase of humidity, and the distribution of water in the SC was also measured. Chemical images provided information about heterogeneous distribution of protein-rich domains and NMF-rich domains. PCA was applied to further enhance images that represent the distribution of each component. It has been found that PCA is particularly useful to extract information, such as the distribution of water in the SC tissue at 95% RH, which is otherwise difficult to obtain. The surface of the SC exposed to liquid ethanol was also studied using ATR-FTIR imaging and a specially designed liquid cell. It has been shown that the distribution of ethanol was homogeneous within the limitations of spatial resolution of our approach. The demonstrated *in situ* imaging approach of ethanol penetration into the SC provides opportunity for further studies of the trans(dermal) drug delivery from the ethanol solutions.

The demonstrated approach is the first step in the applying the ATR-FTIR imaging method to analyze trans(dermal) drug delivery under environmental conditions. Overall, ATR-FTIR imaging should develop into a powerful tool to study and monitor morphological properties of skin and transport behav-

ior through the skin. The implications of this approach may be significant for the development of novel release systems and responsive (for example, to humidity) release systems.

Acknowledgments

We thank EPSRC (Grant EP/D502721/1) for support.

References

1. S. L. Zhang, C. L. Meyers, K. Subramanyan, and T. M. Hancewicz, "Near infrared imaging for measuring and visualizing skin hydration. A comparison with visual assessment and electrical methods," *J. Biomed. Opt.* **10**, 031107 (2005).
2. J. L. Leveque and J. Derigal, "Impedance methods for studying skin moisturisation," *J. Soc. Cosmet. Chem.* **34**, 419–428 (1983).
3. C. W. Blichmann and J. Serup, "Assessment of skin moisture—measurement of electrical conductance, capacitance and transepidemal water-loss," *Acta Derm Venereol* **68**, 284–290 (1988).
4. F. Li, E. Conroy, M. Visscher, and R. Wickett, "The ability of electrical measurements to predict skin moisturization. I. Effects of NaCl and glycerin on short-term measurements, *J. Cosmet. Sci.* **52**, 13–22 (2001).
5. P. J. Caspers, G. W. Lucassen, E. A. Carter, H. A. Bruining, and G. J. Puppels, "*In vivo* confocal Raman microspectroscopy of the skin: noninvasive determination of molecular concentration profiles," *J. Invest. Dermatol.* **116**, 434–442 (2001).
6. P. Xian, J. A. Cowen, and R. E. Imhof, "In-vivo transdermal drug diffusion depth profiling—a new approach to opto-thermal signal analysis," *Anal. Sci.* **17**, 349–352 (2000).
7. P. J. McDonald, A. Akhmerov, L. J. Backhouse, and S. Pitts, "Magnetic resonance profiling of human skin *in vivo* using GARField magnets," *J. Pharm. Sci.* **94**, 1850–1860 (2005).
8. L. Backhouse, M. Dias, J. P. Gorce, J. Hadgraft, P. J. McDonald, and J. W. Wiechers, "GARField magnetic resonance profiling of the ingress of model skin-care product ingredients into human skin in vitro," *J. Pharm. Sci.* **93**, 2274–2283 (2004).
9. E. M. Attas, M. G. Sowa, T. B. Posthumus, B. J. Schattka, H. H. Mantsch, and S. L. Zhang, "Near-IR spectrocoptic imaging for skin hydration: the long and the short of it," *Biopolymers* **67**, 96–106 (2002).
10. E. N. Lewis, P. J. Treado, R. C. Reeder, G. M. Story, A. E. Dowrey, C. Marcott, and I. W. Levin, "Fourier transform spectroscopic imaging using an infrared focal-plane array detector," *Anal. Chem.* **67**, 3377–3381 (1995).
11. C. M. Snively, S. Katzenberger, G. Oskarsdottir, and J. Lauterbach, "Fourier-transform infrared imaging using a rapid-scan spectrometer," *Opt. Lett.* **24**, 1841–1843 (1999).
12. S. G. Kazarian, K. L. A. Chan, V. Maquet, and A. R. Boccaccini, "Characterisation of bioactive and resorbable polyactide/bioglass® composites by FTIR spectroscopic imaging," *Biomaterials* **25**, 3931–3938 (2004).
13. I. W. Levin and R. Bhargava, "Fourier transform infrared vibrational spectroscopic imaging: integrating microscopy and molecular recognition," *Annu. Rev. Phys. Chem.* **56**, 429–474 (2005).
14. S. G. Kazarian and K. L. A. Chan, "Applications of ATR-FTIR spectroscopic imaging to biomedical samples," *Biochim. Biophys. Acta* **1758**, 858–867 (2006).
15. N. J. Harrick, *Internal Reflection Spectroscopy*, Harrick Scientific Corporation, New York (1987).
16. K. L. A. Chan and S. G. Kazarian, "New opportunities in micro- and macro-attenuated total reflection infrared spectroscopic imaging: spatial resolution and sampling versatility," *Appl. Spectrosc.* **57**, 381–389 (2003).
17. S. G. Kazarian and K. L. A. Chan, "'Chemical photography' of drug release," *Macromolecules* **36**, 9866–9872 (2003).
18. K. L. A. Chan and S. G. Kazarian, "ATR-FTIR spectroscopic imaging with expanded field of view to study formulations and dissolution," *Lab Chip* **6**, 864–870 (2006).
19. E. M. Burka and R. Curbelo, Imaging ATR Spectrometer, U.S. Patent 6,414,100 (2000).
20. K. L. A. Chan and S. G. Kazarian, "Macro FTIR imaging in transmission under a controlled environment," *Vib. Spectrosc.* **42**, 130–134 (2006).
21. B. O. Budevska, S. T. Sum, and T. J. Jones, "Application of multivariate curve resolution for analysis of FT-IR microspectroscopic images of in situ plant tissue," *Appl. Spectrosc.* **57**, 124–131 (2003).
22. J. van der Weerd and S. G. Kazarian, "Combined approach of FTIR imaging and conventional dissolution tests applied to drug release," *J. Controlled Release* **98**, 295–305 (2004).
23. K. L. A. Chan and S. G. Kazarian, "Visualisation of the heterogeneous water sorption in a pharmaceutical formulation under controlled humidity via FT-IR imaging," *Vib. Spectrosc.* **35**, 45–49 (2004).
24. S. M. Harrison, B. W. Barry, and P. H. Dugard, "Effect of freezing on human skin permeability," *J. Pharm. Pharmacol.* **36**, 261–262 (1984).
25. K. L. A. Chan and S. G. Kazarian, "Fourier transform infrared imaging for high-throughput analysis of pharmaceutical formulations," *J. Comb. Chem.* **7**, 185–189 (2005).
26. K. L. A. Chan, S. V. Hammond, and S. G. Kazarian, "Applications of attenuated total reflection infrared spectroscopic imaging to pharmaceutical formulations," *Anal. Chem.* **75**, 2140–2146 (2003).
27. J. E. Harrison, A. C. Watkinson, D. M. Green, J. Hadgraft, and K. Brian, "The relative effect of Azone and Transcutol on permeant diffusivity and solubility in human stratum corneum," *Pharm. Res.* **13**, 542–546 (1996).
28. S. Ekgasit and A. Padermshoke, "Optical contact in ATR/FT-IR spectroscopy," *Appl. Spectrosc.* **55**, 1352–1359 (2001).
29. K. L. A. Chan and S. G. Kazarian, "Attenated total reflection FTIR imaging with variable incident angles: a 3-D profiling of heterogeneous materials," *Appl. Spectrosc.* **61**, 48–54 (2007).
30. P. Garidel, "Mid-FTIR-microspectroscopy of stratum corneum single cells and stratum corneum tissue," *Phys. Chem. Chem. Phys.* **4**, 5671–5677 (2002).
31. I. R. Scott and C. R. Harding, "Filaggrin breakdown to water binding-compounds during development of the rat stratum-corneum is controlled by the water activity of the environment," *Dev. Biol.* **115**, 84–92 (1986).
32. G. Zhang, D. J. Moore, R. Mendelsohn, and C. R. Flach, "Vibrational microspectroscopy and imaging of molecular composition and structure during human corneocyte maturation," *J. Invest. Dermatol.* **126**, 1088–1094 (2006).
33. R. Salzer, G. Steiner, H. H. Mantsch, J. Mansfield, and E. N. Lewis, "Infrared and Raman imaging of biological and biomimetric samples," *Fresenius' J. Anal. Chem.* **366**, 712–726 (2000).
34. K. L. A. Chan, N. Elkhider, and S. G. Kazarian, "Spectroscopic imaging of compacted pharmaceutical tablets," *Chem. Eng. Res. Des.* **83**, 1303–1310 (2005).
35. N. Labbe, T. G. Rials, S. S. Kelley, Z. M. Cheng, J. Y. Kim, and Y. Li, "FT-IR imaging and pyrolysis-molecular beam mass spectrometry: new tools to investigate wood tissues," *Wood Sci. Technol.* **39**, 61-U19 (2005).
36. J. Van der Weerd and S. G. Kazarian, "Release of poorly soluble drugs from HPMC tablets studied by FTIR imaging and flow-through dissolution tests," *J. Pharm. Sci.* **94**, 2096–2109 (2005).
37. J. Van der Weerd, "Combined approach of FTIR imaging and conventional dissolution tests applied to drug release," *J. Controlled Release* **98**, 295–305 (2004).
38. I. H. McColl, E. W. Blanch, L. Hecht, and L. D. Barron, "A study of alpha-helix hydration in polypeptides, proteins, and viruses using vibrational Raman optical activity," *J. Am. Chem. Soc.* **126**, 8181–8188 (2004).
39. R. Schweitzer-Stenner, "Advances in vibrational spectroscopy as a sensitive probe of peptide and protein structure—a critical review," *Vib. Spectrosc.* **42**, 98–117 (2006).
40. D. W. Rafferty and J. L. Koenig, "FTIR imaging for the characterization of controlled-release drug delivery applications," *J. Controlled Release* **83**, 29–39 (2002).
41. A. Gupper and S. G. Kazarian, "Study of solvent diffusion and solvent-induced crystallization in syndiotactic polystyrene using FT-IR spectroscopy and imaging," *Macromolecules* **38**, 2327–2332 (2005).